



# Annual patterns in phytoplankton phenology in Antarctic coastal waters explained by environmental drivers

Maria A. van Leeuwe<sup>1b</sup>,<sup>1\*</sup> Alison L. Webb,<sup>1,a</sup> Hugh J. Venables,<sup>2</sup> Ronald J.W. Visser,<sup>3</sup> Mike P. Meredith,<sup>2</sup> J. Theo M. Elzenga,<sup>1</sup> Jacqueline Stefels<sup>1</sup>

<sup>1</sup>University of Groningen, GELIFES, Groningen, The Netherlands

<sup>2</sup>British Antarctic Survey, Cambridge, United Kingdom

<sup>3</sup>University of Groningen, ESRIG, Groningen, The Netherlands

## Abstract

Coastal zones of Antarctica harbor rich but highly variable phytoplankton communities. The mechanisms that control the dynamics of these communities are not well defined. Here we elucidate the mechanisms that drive seasonal species succession, based on algal photophysiological characteristics and environmental factors. For this, phytoplankton community structure together with oceanographic parameters was studied over a 5-year period (2012–2017) at Rothera Station at Ryder Bay (Western Antarctic Peninsula). Algal pigment patterns and photophysiological studies based on fluorescence analyses were combined with data from the Rothera Time-Series program. Considerable interannual variation was observed, related to variations in wind-mixing, ice cover and an El Niño event. Clear patterns in the succession of algal classes became manifest when combining the data collected over the five successive years. In spring, autotrophic flagellates with a high light affinity were the first to profit from increasing light and sea ice melt. These algae most likely originated from sea-ice communities, stressing the role of sea ice as a seeding vector for the spring bloom. Diatoms became dominant towards summer in more stratified and warmer surface waters. These communities displayed significantly lower photoflexibility than spring communities. There are strong indications for mixotrophy in cryptophytes, which would explain much of their apparently random occurrence. Climate models predict continuing retreat of Antarctic sea-ice during the course of this century. For the near-future we predict that the marginal sea-ice zone will still harbor significant communities of haptophytes and chlorophytes, whereas increasing temperatures will mainly be beneficial for diatoms.

The Antarctic coastal zones belong to the most productive areas of the planet, and play a very important role in marine biogeochemical cycles (Arrigo et al. 2017; Steiner and Stefels 2017). The Western Antarctic Peninsula (WAP) is such a hot spot for primary production. In spring and summer, algal blooms may develop to concentrations of  $> 20 \mu\text{g Chl } a \text{ L}^{-1}$  (Vernet et al. 2008; Kim et al. 2018). These blooms support a rich food web including krill and fish, culminating in charismatic species like penguins, seals and whales (Moline et al. 2004; Saba et al. 2014). Microalgae furthermore play an important role in biogeochemical cycles and climate processes through the uptake of  $\text{CO}_2$  (Legge et al. 2017) and the production of various climate active gases like dimethylsulfide (Stefels et al. 2018; Webb et al. 2019)

and halocarbons (Hughes et al. 2009). Algal growth at the WAP is supported by ample supply of macro- and micronutrients due to glacial input and the intrusion of upper circumpolar deep water (UCDW), and a stable light climate is provided by summer stratification due to solar heating and wind shelter in bay areas (Clarke et al. 2008; Vernet et al. 2008; Annett et al. 2017; Bown et al. 2018).

Global warming is affecting the polar regions more than any region on earth. The WAP underwent rapid climate change during the second half of the twentieth century, with increasing atmospheric temperatures, and strong rises in temperatures of surface and deep waters, associated with a decline in sea-ice cover (Meredith and King 2005; Stammerjohn et al. 2008). More recently, atmospheric temperatures have stabilized and even decreased in some WAP locations, attributed to natural interannual variability in atmospheric circulation (Turner et al. 2016), though warming here and around the rest of Antarctica is predicted during the 21st century under the increasing influence of greenhouse gases (Meijers 2014). The impact of these changes on the algal

\*Correspondence: m.a.van.leeuwe@rug.nl

This is an open access article under the terms of the Creative Commons Attribution-NonCommercial-NoDerivs License, which permits use and distribution in any medium, provided the original work is properly cited, the use is non-commercial and no modifications or adaptations are made.

<sup>a</sup>Present address: University of Warwick, Coventry, United Kingdom

community structure is not well known and predictions are difficult without a conceptual framework that relates patterns of seasonal species succession to environmental drivers. Since changes in algal biomass and community composition will affect all higher trophic levels and have an influence on the full ecosystem a better understanding is required (Deppeler and Davidson 2017; Henley et al. 2019).

Algal growth in the southern latitudes is distinct for its strong seasonality in production driven by the annual solar cycle (Clarke et al. 2008; Ducklow et al. 2012). In spring, algal growth is activated by increasing light availability with growing daylight and higher solar angle. The formation of a stable thin surface layer of low-density seawater associated with sea-ice melt furthermore supports the development of algal blooms. The spring bloom is a persistent feature at the WAP. Over the course of summer, stratification of surface waters provides favorable conditions for the development of algal blooms (Clarke et al. 2008; Venables et al. 2013). The magnitude of the summer bloom at the WAP appears to be influenced by ice conditions in the preceding winter. Reduced sea-ice cover in winter results in deep mixing of the water column and, consequently more (solar) energy is required to stabilize the water column the following summer, compared to a summer following strong ice conditions and accordingly weak wind mixing of the water column (Venables et al. 2013). Concomitantly more algal biomass can build-up in more stratified waters, which ultimately results in large phytoplankton blooms.

The annual variations in biomass are accompanied by strong dynamics in algal community structure. In winter, algal biomass is generally low and dominated by small picoplankton (Clarke et al. 2008; Rozema et al. 2017a). Summer communities are mostly dominated by diatoms (Schofield et al. 2017; Rozema et al. 2017a), but large blooms of *Phaeocystis antarctica* have also been observed (Annett et al. 2010). Moreover, in recent decades, cryptophytes are more frequently observed (Montes-Hugo et al. 2009; Schofield et al. 2017). The mechanisms that regulate the algal phenology are still poorly defined due to a lack of dedicated studies. Our knowledge on algal abundance and seasonal succession is mainly based on field studies that link species occurrence with oceanographic conditions and from which general patterns emerge. The signature of the spring bloom is partly determined by sea-ice algal communities that may seed the phytoplankton community (van Leeuwe et al. 2018). Secondly, light conditions are an important factor that may drive population dynamics; photophysiological characteristics vary for each algal group (Richardson et al. 1983; van Leeuwe et al. 2005). Summer blooms are mostly dominated by diatoms that benefit from a stable light climate as it occurs later in the season (Arrigo et al. 1999). In addition, temperature is a discriminating factor, with differential growth preference for various algal species. A lower temperature preference for *Phaeocystis* compared to diatoms was established in the Ross Sea (Liu and Smith 2012). In the northern section of the WAP, cold waters

appear to be most favorable for cryptophytes (Schofield et al. 2017), but uncertainties remain as to the growth preferences of this group (Mendes et al. 2013).

In this paper we present an extensive study on algal composition in the WAP and its driving factors. The phytoplankton community and its associated photophysiological characteristics were studied at Ryder Bay and linked to the Rothera Time-Series (RaTS; Clarke et al. 2008), a multi-decade sustained observational program at the WAP that includes wintertime measurements. Ryder Bay makes an ideal natural laboratory as the phytoplankton community composition is highly dynamic and contains both diatoms as well as various classes of flagellates, including the haptophyte *P. antarctica*, an eminent player in the WAP area (Annett et al. 2010; Rozema et al. 2017a). The physical oceanography in Ryder Bay has been studied intensively over the last decades, which provided a firm background for data analyses (see Stefels et al. 2017). In addition to previous work on phytoplankton dynamics (Rozema et al. 2017a), our study had a strong focus on phytoplankton photophysiological characteristics that may explain the succession of algal classes from a mechanistic perspective. Our study continued over five consecutive years, and extended over both winter and summer. During this period the transition from winter to spring communities was well covered. Clear trends in succession of algal classes and linkages with its driving parameters were revealed. In this paper, we connect the insights learned at Ryder Bay with a collection of previous observations in the Antarctic coastal zone (a.o. Arrigo et al. 1999; Garibotti et al. 2005; Schloss et al. 2012; Rozema et al. 2017a; Schofield et al. 2017; Henley et al. 2019). The elucidation of mechanisms that drive algal phenology provides us with a conceptual framework that we apply for a prediction of near-future changes of phytoplankton dynamics in Antarctic coastal areas.

## Material and methods

### Sampling

Samples were taken over 5 consecutive years (January 2013–March 2017) from the RaTS site at 67.570°S, 68.225°W in Ryder Bay (Fig. 1), a southeast-facing embayment of Adelaide Island at the northern end of Marguerite Bay, WAP. In the summer season (November–March), seawater samples were taken over the full depth profile, preferably twice a week. In winter (April–October), sampling was limited to 15 m and the frequency restricted by ice and wind conditions. In total, 89 stations were sampled in summer and 57 stations sampled in winter.

Discrete samples were collected from the water column at 5, 15, 25, and 40 m with Niskin-bottles and a hand winch from a small boat. Surface water was sampled by hand with a 10-liter Nalgene bottle. Alongside the seawater sampling, a Seabird 19+ conductivity, temperature, and depth (CTD) instrument was deployed, combined with a WetLabs in-line fluorometer and LiCOR photosynthetically active radiation (PAR) sensor for collection of general oceanographic data. Samples were stored in the dark and at ambient temperature

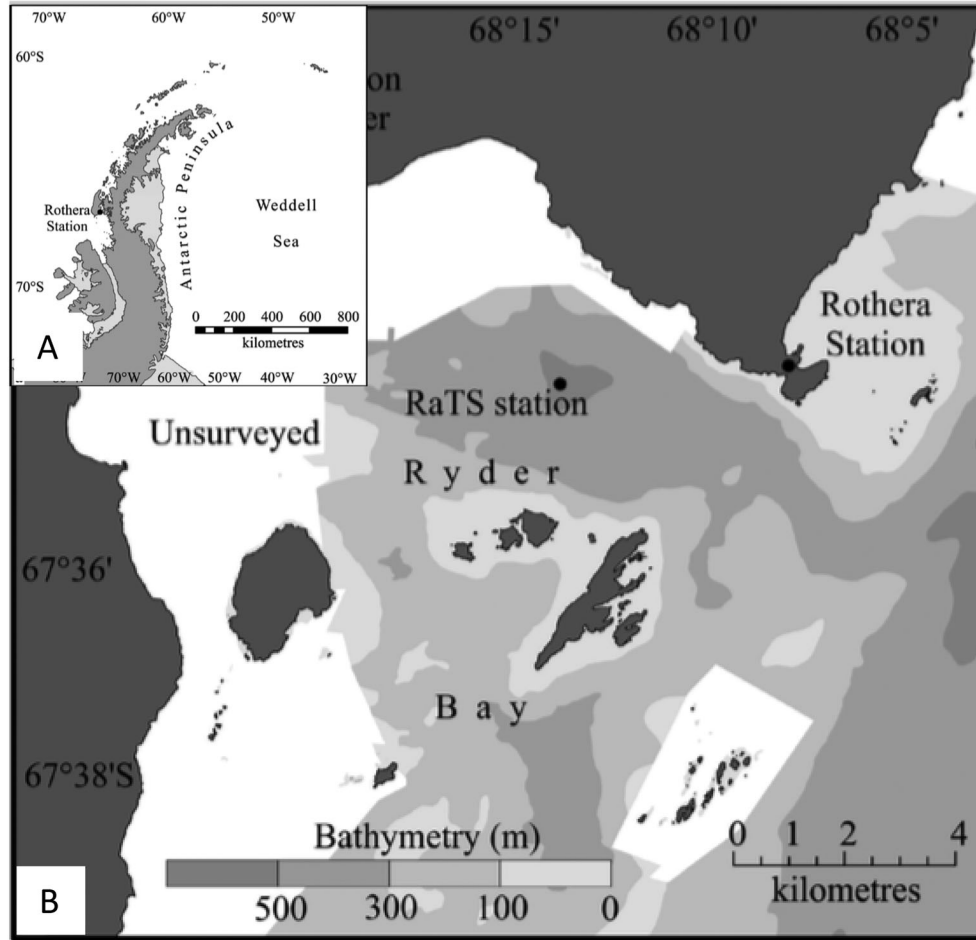


**Fig. 1.** Location of the British research station Rothera at the Western Antarctic Peninsula (a) and the RaTS sampling station located in Ryder Bay (b).

for return to the laboratory, where subsamples were taken for nutrients, algal pigments and fluorescence analyses (spring and summer samples only). In the two consecutive summers of 2012/2013 and 2013/2014, samples were also taken for microscopic cell counts. In addition, samples were taken for dimethylsulfide and dimethylsulfoniopropionate, which is discussed in accompanying papers (Stefels et al. 2018; Webb et al. 2019).

### Collection of oceanographic parameters

Seawater density derived from the CTD was used to calculate the mixed layer depth (MLD), defined here as the depth where the potential density exceeds that at the surface by  $0.05 \text{ kg m}^{-3}$  (Venables et al. 2013). Sea-ice observations are an integral part of the RaTS science program (for details on data collection and data availability, see <https://www.bas.ac.uk/project/rats/>). Sea-ice cover in the bay was evaluated visually on a daily basis by observers on station: zero visible open water characterized 100% sea ice cover, and 0% was no visible ice.

The solar radiation dose (SRD,  $\text{W m}^{-2}$ ) over the MLD was calculated as a function of sea-ice cover, irradiance (measured at Rothera Point by a Sky Instruments SKP215 in  $\mu\text{mol m}^{-2} \text{ s}^{-1}$ ), solar angle  $I_o$  and the diffuse attenuation coefficient  $k$  (Vallina and Simo 2007):

$$\text{SRD} = \frac{I_o}{k \times \text{MLD}} \times (1 - e^{-k \times \text{MLD}}) \quad (1)$$

Meteoric water (glacial discharge and precipitation) was determined based on  $\delta^{18}\text{O}$ , the standardized ratio of the stable isotopes of oxygen in seawater (see Meredith et al. 2017 for details).

### Chlorophyll fluorescence parameters

Photosynthetic performance was assessed on samples collected between November and March, using a pulse-amplitude-modulated (PAM) fluorometer (Water PAM, Heinz Walz, GmbH). Recordings that required gain settings  $>10$  were ignored as such high settings were observed to pose a positive bias on yield values. After arrival at the laboratory fluorescence

analyses was started immediately. Prior to each analysis, subsamples were dark-adapted for 10 minutes. Rapid light curves were established by 30 seconds exposure to 0, 10, 40, 70, 110, 160, 220, 290, 350, and 400  $\mu\text{mol photons m}^{-2} \text{s}^{-1}$ . The first recording of the light curves provides the maximum quantum yield of photosynthesis (Fv/Fm). The maximum rate of electron transport  $P_{\text{max}}$  ( $\mu\text{mol electrons m}^{-2} \text{s}^{-1}$ ) and light affinity  $\alpha$  ( $\text{electrons photon}^{-1} \text{m}^{-2} \text{s}^{-1}$ ) were determined using a nonlinear fit (Prism) based on the photosynthesis-irradiance equation by Platt et al. (1980).

Induction curves were established to determine the effective quantum yield of photosynthesis ( $Y_{\text{eff}}$ ) and recovery capacity ( $\text{IC}_{\text{Rec}}$ ). Ambient communities were exposed to 40  $\mu\text{mol photons m}^{-2} \text{s}^{-1}$  for 10 min, using the internal light source of the PAM fluorometer. Recovery following exposure was recorded during 10 min in the dark;  $Y_{\text{eff}}$  and  $\text{IC}_{\text{Rec}}$  were determined by a nonlinear fit in Prism.

In addition, light shock experiments were performed to further test the capacity for photoacclimation. Across all years, 4 shock experiments were executed in November, 9 in December, 15 in January and 2 in February. For these experiments, a set of 3 mL subsamples was placed outdoors in the snow, and exposed to near surface irradiance ( $\sim 1000 \mu\text{mol photons m}^{-2} \text{s}^{-1}$ ) for 60 min. In case of high irradiance, the samples were screened with mesh, allowing UV to penetrate. Light intensities were recorded with a BioSpherical Instruments 3 pi sensor. After exposure, samples were placed indoors at 4°C at low light ( $\sim 20 \mu\text{mol photons m}^{-2} \text{s}^{-1}$ ). Recovery of the quantum yield was recorded by regular recordings of Fv/Fm over a period of 2 h; the duration of recovery  $K_{\text{m}}$  (min) was determined by a nonlinear fit in Prism.

### Nutrient analyses

Samples were filtered (0.2  $\mu\text{m}$  discs, Whatman PLC, United Kingdom) and stored at  $-20^\circ\text{C}$  (nitrate plus nitrite, phosphate) or  $+4^\circ\text{C}$  (silicic acid) until analyses, using a Technicon TRAACS 800 Autoanalyzer (Bran and Luebbe) following standard methods (Grasshoff 1983). Detection limits were 0.01, 0.02, and 0.26  $\mu\text{M}$  for phosphate, nitrate plus nitrite, and silicic acid, respectively.

### Pigment analyses

A sample volume between 2 and 6 liter was filtered gently ( $< 15 \text{ kPa}$ ) over a GF/F filter (Whatman), subsequently snap-frozen in liquid nitrogen and stored at  $-80^\circ\text{C}$  until analysis. Before extraction in 90% acetone, filters were freeze-dried at  $-50^\circ\text{C}$ , over 48 h. Pigments were analyzed by high-performance liquid chromatography (HPLC) on a Waters 2695 system equipped with a 996 photodiode array detector (van Heukelem and Thomas 2001; van Leeuwe et al. 2006), using a Zorbax C8, 3.5  $\mu\text{m}$  column. Pigment standards were obtained from DHI Water Quality Institute (Horsholm, Denmark).

Pigment ratios to chlorophyll *a* (Chl *a*) were used to discern trends over the full five consecutive years. A CHEMTAX matrix factorization was applied to summer communities to

derive algal classes from pigment patterns (Wright et al. 1996). Sampling frequency in winter was too low to allow for accurate CHEMTAX analyses. Summer data were analyzed for each season separately, using a similar input matrix for all summer seasons (Table 1). The water column was separated in two layers ("bins" in CHEMTAX): above and below 15 m (Table 1).

The initial pigment ratio included eight algal classes. These classes were chosen based on previous results and literature information (e.g. Wright et al. 2010; van Leeuwe et al. 2015; Rozema et al. 2017a) and microscopy. Two groups of diatoms were described: Diatoms\_1 contained typical diatom species like *Chaetoceros* sp. and *Coscinodiscus* sp. that are characterized by Chl *c1*, and Chl *c2*; Diatoms\_2 is a separate group in which Chl *c1* is replaced by Chl *c3*. The latter group represents *Pseudo-nitzschia* sp., though not exclusively. Haptophytes were also separated in two groups, "C" and "P." Microscope observations showed that Haptophyceae\_C mainly consisted of *Chrysomonodales*. The input ratios for Haptophyceae\_P were based on pigment ratios typical for *P. antarctica* (van Leeuwe et al. 2014). The presence of *P. antarctica* was also confirmed by microscopy. Haptophyceae\_P did not exclusively refer to *Phaeocystis*. Dinoflagellates were described as a separate class based on the presence of peridinin. However, as many dinoflagellates do not carry peridinin, but contain a variety of pigments, this is a very difficult group to identify (see Wright et al. 2010). Chlorophytes are defined by Chl *b*. This group may also include prasinophytes. Cryptophytes were based on the presence of alloxanthin.

### Cell counts

For the determination of species composition and abundance, 100 ml seawater subsamples were taken from 5 and 15 m depth, and subsequently preserved in a 0.5% lugol solution for analysis at the University of Helsinki (Finland). Cell counts were performed with an inverted microscope (Olympus IMT-2), after sedimentation in a cuvette according to Utermohl (1958). Cell abundance was calculated as percentage of total cells per station and accounted for occurrence throughout the season.

### Statistical analyses

To establish significant differences between months, oceanographic and biological data were analyzed by One-way ANOVA followed by Bonferroni's comparison test. All data did meet the assumptions of normality and homoscedasticity, except for the CTD-data that were  $\log_{10}$ -transformed before analyses. To establish relations between algal classes and various oceanographic and photophysiological parameters, data were first analyzed by linear modeling (RStudio, 0.99.902). The most plausible model prediction was achieved by reducing the numbers of variables by applying Akaike Information Criteria. Canonical correspondence analysis (CCA) was then performed (RStudio, 0.99.902, Vegan package) to depicture the relationship between the community composition as

**Table 1.** Input ratios for Chemtax analyses for all five seasons, with two bins distinguished. For the summer season of 2013, neoxanthin was excluded from the matrix. For 2015, prasinoxanthin was excluded.

Class	Chl c2	Peri	Fuco	Hex-kfuco	Hex-fuco	Neo	Prasino	Allo	Chl b
0–15 m									
Prasinophytes	0	0	0	0	0	0.007	0.016	0	0.050
Dinoflagellates	0	1.069	0	0	0	0	0	0	0
Cryptophytes	0.100	0	0	0	0	0	0	0.300	0
Haptophytes_P	0.420	0	0.800	0.500	0.298	0	0	0	0
Haptophytes_C	0	0	0.104	0	0.459	0	0	0	0
Chlorophytes	0	0	0	0	0	0.045	0	0	0.464
Diatoms_1	0.300	0	0.506	0	0	0	0	0	0
Diatoms_2	0	0	0.886	0	0	0	0	0	0
15–40 m									
Prasinophytes	0	0	0	0	0	0.037	0.277	0	0.174
Dinoflagellates	0	2.224	0	0	0	0	0	0	0
Cryptophytes	0.253	0	0	0	0	0	0	0.675	0
Haptophytes_P	0.305	0	1.000	0.500	0.582	0	0	0	0
Haptophytes_C	0	0	0.100	0	0.465	0	0	0	0
Chlorophytes	0	0	0	0	0	0.045	0	0	0.471
Diatoms_1	0.300	0	0.560	0	0	0	0	0	0
Diatoms_2	0	0	0.903	0	0	0	0	0	0

calculated with CHEMTAX and respectively environmental and photophysiological parameters. For the first CCA, environmental parameters initially tested included nitrate, silicic acid, phosphate, salinity, temperature, density, MLD, PAR, and SRD. Missing values for PAR and phosphate were interpolated as average values between adjacent sample days. For the second CCA-analyses, photophysiological parameters tested included  $F_v/F_m$ ,  $P_{max}$ ,  $\alpha$ ,  $Y_{eff}$ ,  $IC_{Rec}$  and  $K_m$ .

## Results

### Oceanography

During all winters, Ryder Bay experienced 100% sea-ice cover for a minimum of three weeks in 2013 to a maximum of 16 weeks in 2016. Sea ice broke up between October and December (Fig. 2). With the onset of spring, the 15m surface temperature gradually increased from a mean of  $-1.5^\circ\text{C}$  over during winter to a maximum daily mean of  $0.48^\circ\text{C}$  in February (Table 2). From October onwards, rising temperatures and increasing PAR were associated with a decline in salinity and density of surface waters (Fig. 2), which indicated substantial ice melt. The seasonal warming of the water column, and ensuing deepening of low-density signals were mirrored in a shallowing of the mixed layer, with shallowest layers in January (Table 2). Simultaneously, the SRD reached highest values in January (Table 2). In most years two algal blooms were discerned; the break-up of the ice sheet in early spring triggered the first bloom (Fig. 2). A second bloom occurred in summer (February-March).

Over the five years sampled, significant departures from the mean seasonal progression described above were observed. Firstly, the duration of ice cover increased with each progressive winter. Secondly, marked interannual variability of MLD and the UCDW temperature at 100m was observed. The winters of 2015 and 2016 had shallow mixed layers and high temperatures at 80-100m. The following season was marked by persistent ice cover, with Ryder Bay remaining covered by sea ice until early 2017. The rapid break-up of sea ice in January 2017 subsequently resulted in very low salinity and density surface waters (Fig. 2). The surface waters supported highest algal biomass over the 5-year record with Chl *a* concentrations  $> 30 \mu\text{g L}^{-1}$ . In contrast, Chl *a* concentrations remained low in 2015/2016 with few values  $> 10 \mu\text{g Chl } a \text{ L}^{-1}$ .

Due to algal consumption, concentrations of all nutrients dropped over summer (Fig. 3), with lowest surface values of less than  $1 \mu\text{M NO}_3$  and  $0.1 \mu\text{M PO}_4$  recorded in January and February 2017 (Table 2) and the strongest decline in Si concentrations in summer 2014. During autumn and winter, cooling of the water column resulted in mixing of surface waters with deeper layers. Nutrients were consequently replenished, as reflected in elevated spring concentrations of  $\text{NO}_3$ ,  $\text{PO}_4$ , and Si (Fig. 3).

### Phytoplankton community structure

The pigment signature of the algal communities varied over time (Fig. 4). Fucoxanthin (Fuco) closely followed the Chl *a* pattern with high concentrations in the summers of 2013 and 2017. Concentrations of 19'-hexanoyloxyfucoxanthin (Hexa) and 19'-hexanoyloxy-4-ketofucoxanthin (Keto) were

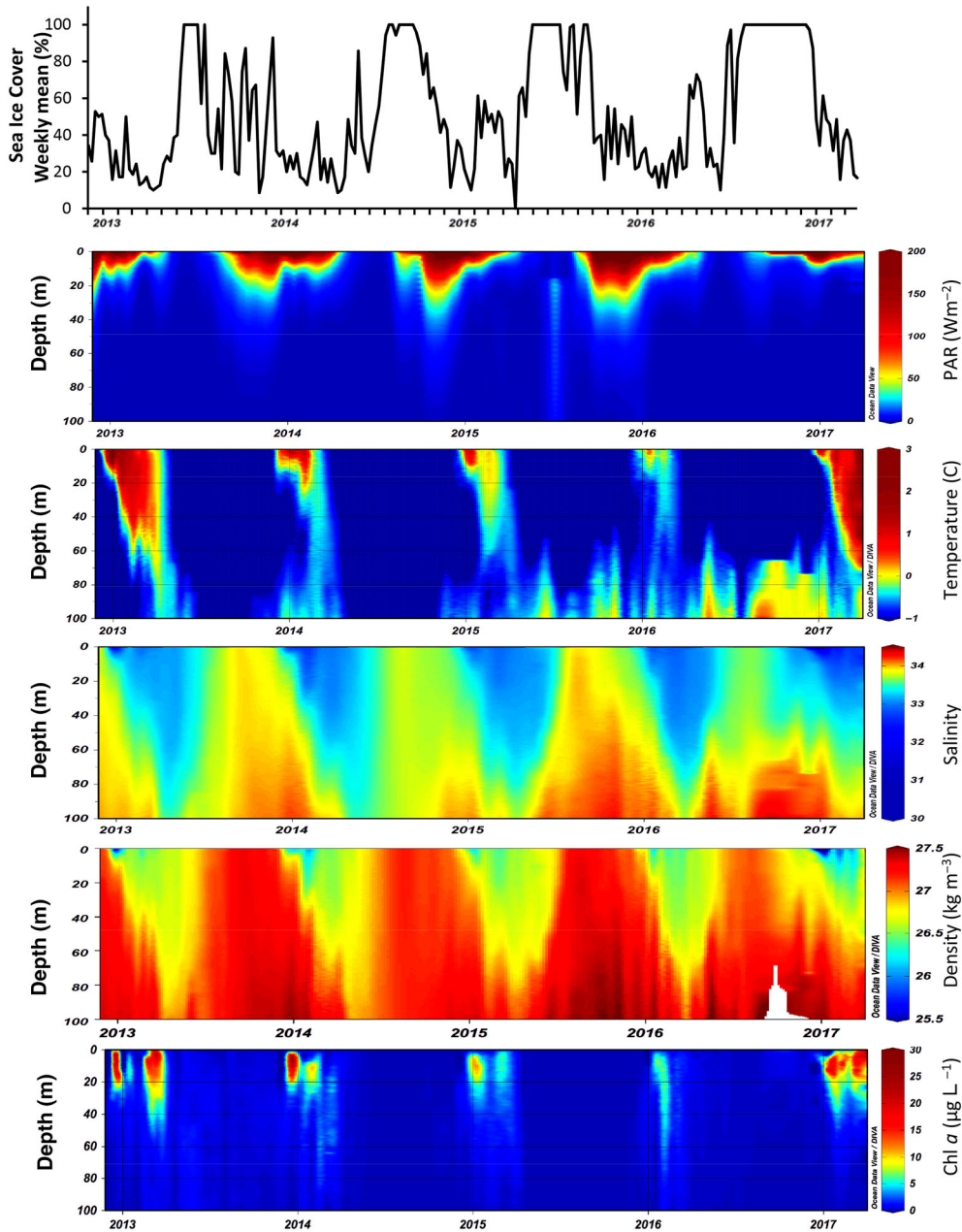


**Fig. 2.** Time series of sea-ice cover, PAR, temperature, salinity, density, and Chl *a* for the top 100 m. PAR, temperature and salinity were recorded by CTD-instruments. Chl *a* was derived from the fluorometer attached to the CTD.

opposite to Fuco with highest concentration in 2014 and 2015. Concentrations of 19'-butanoyloxyfucoxanthin (Buta) were more variable, just like chlorophyll *b* (Chl *b*) and alloxanthin (Allo) concentrations. The very high concentration of  $> 2 \mu\text{g Chl } b \text{ L}^{-1}$  recorded in March 2016 and January 2017 are noteworthy. The companion increases in neoxanthin (Neo) reflect anomalously high concentration of distinct phytoplankton species. Likewise, prasinoloxanthin (Prasino) concentrations were increased in 2016 and 2017, especially at 25 and 40 m.

A clear seasonality in pigment patterns was observed when all data were pooled together (Fig. 5). High Chl *a* concentrations combined with high ratios of Fuco/Chl *a* marked the summer blooms in December–March. With declining Chl *a* concentration from March onwards, Fuco/Chl *a* dropped whereas Hexa/Chl *a* and Keto/Chl *a* increased (Fig. 5), reflecting the rise of autotrophic flagellates. In winter, prasinophytes and chlorophytes were most abundant, as indicated by the higher ratios in Buta, Chl *b*, Neo, and Pras to Chl *a* (Fig. 5). Cryptophytes, marked by Allo/Chl *a*, were also present in mid-winter, but reached maximum

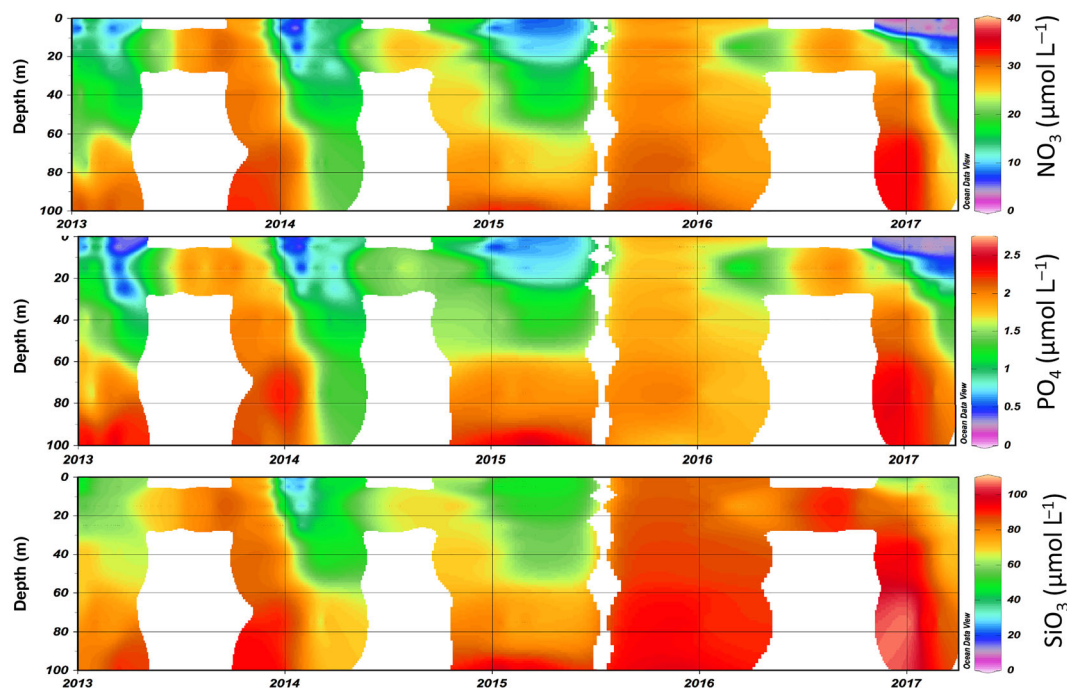
**Table 2.** Oceanographic and biological parameters (av, min, max) for Ryder Bay, recorded at 15 m over five consecutive years between 2012 and 2017.

	Nov	Dec	Jan	Feb	Mar
Temperature (°C)*	-1.52 (-1.72, -0.96)	-0.43 (-1.51, 1.59)	0.45 (-0.83, 2.31)	0.48 (-0.77, 2.31)	-0.06 (-10.01, 1.23)
Salinity*	33.64 (33.11, 33.86)	33.41 (32.61, 33.73)	33.03 (32.24, 33.66)	32.93 (32.24, 33.66)	32.93 (32.62, 33.15)
Density (kg m <sup>-3</sup> )*	27.08 (26.65, 27.25)	26.85 (26.22, 27.13)	26.49 (25.86, 27.06)	26.41 (25.86, 27.06)	26.45 (26.16, 26.72)
SRD (μmol photons m <sup>-2</sup> s <sup>-1</sup> )	20.4 (0.3, 75.7) <sup>a</sup>	37.2 (1.1, 156.8) <sup>b</sup>	39.2 (2.5, 110.7) <sup>b</sup>	17.9 (1.1, 81.1) <sup>a</sup>	5.4 (0.2, 33.3) <sup>c</sup>
MLD (m)	21.80 (4, 53) <sup>a</sup>	4.94 (1, 34) <sup>b</sup>	4.11 (1, 18) <sup>b</sup>	12.69 (1, 39) <sup>a</sup>	17.6 (1, 55) <sup>a</sup>
Nitrate (μmol L <sup>-1</sup> )	29.11 (28.49, 29.86) <sup>a</sup>	21.35 (3.40, 30.65) <sup>a</sup>	10.78 (1.04, 28.11) <sup>b</sup>	9.40 (0.12, 19.47) <sup>c</sup>	8.84 (2.20, 15.24) <sup>c</sup>
Phosphate (μmol L <sup>-1</sup> )	1.76 (1.74, 1.78) <sup>a</sup>	1.35 (0.18, 2.02) <sup>a</sup>	0.74 (0.08, 1.98) <sup>b</sup>	0.65 (0.03, 1.29) <sup>b</sup>	0.53 (0.10, 1.23) <sup>b</sup>
Silicate (μmol L <sup>-1</sup> )	79.86 (77.21, 82.46) <sup>a</sup>	69.68 (4.78, 87.17) <sup>a</sup>	56.55 (15.82, 89.11) <sup>a</sup>	51.42 (15.02, 67.36) <sup>b</sup>	55.66 (44.95, 61.73) <sup>b</sup>
Chl <i>a</i> (μg L <sup>-1</sup> )*	0.40 (0.35, 0.49)	3.98 (0.18, 19.89)	7.99 (0.83, 32.91)	9.38 (0.76, 23.12)	14.48 (0.95, 28.31)
Fv/Fm	0.69 (0.46, 0.78) <sup>a</sup>	0.61 (0.43, 0.82) <sup>b</sup>	0.56 (0.33, 0.74) <sup>c</sup>	0.62 (0.51, 0.73) <sup>a, b</sup>	0.63 (0.57, 0.69) <sup>a, b, c</sup>
Y <sub>eff</sub>	0.53 (0.36, 0.69) <sup>a</sup>	0.42 (0.21, 0.85) <sup>b</sup>	0.33 (0.11, 0.58) <sup>c</sup>	0.42 (0.16, 0.55) <sup>a, b</sup>	0.49 (0.43, 0.55) <sup>a, b</sup>
IC <sub>Rec</sub> (min)	0.89 (0.68, 1.15) <sup>a</sup>	1.15 (0.55, 2.13) <sup>a, b</sup>	0.98 (0.28, 2.10) <sup>a, c</sup>	1.37 (0.33, 2.16) <sup>b</sup>	1.40 (1.03, 2.01) <sup>a, c</sup>
K <sub>m</sub> (min)	6.13 (0.10, 53.24) <sup>a</sup>	6.91 (0.94, 23.99) <sup>a</sup>	20.74 (0.88, 81.78) <sup>b</sup>	22.56 (3.47, 97.65) <sup>a</sup>	n.d.

\*Significant differences between all months (ANOVA;  $p < 0.001$ ); treatments with different letters are significantly different ( $p < 0.05$ ); for abbreviations, see text.

abundances in January (Figs. 5, 6). Haptophytes were the first to increase again in spring, with rapidly increasing ratios of Hexa/Chl *a* starting in September. Peridinin/Chl *a* ratios were highly variable. Peridinin indicates the presence of dinoflagellates, but this group is very difficult to accurately quantify based on pigment analyses.

The ratio of pheophorbide/Chl *a*, a measure of heterotrophic activity, was highly variable due to erratic biomass present in winter (Fig. 5). High ratios were recorded mostly in autumn and midwinter. Ratios of diato-plus diadinoxanthin (dt + dd) to Chl *a* were high in summer (December–January),

**Fig. 3.** Time series of nitrate, phosphate and silicic acid. Sampling for nutrients in winter time was limited to 15 m.

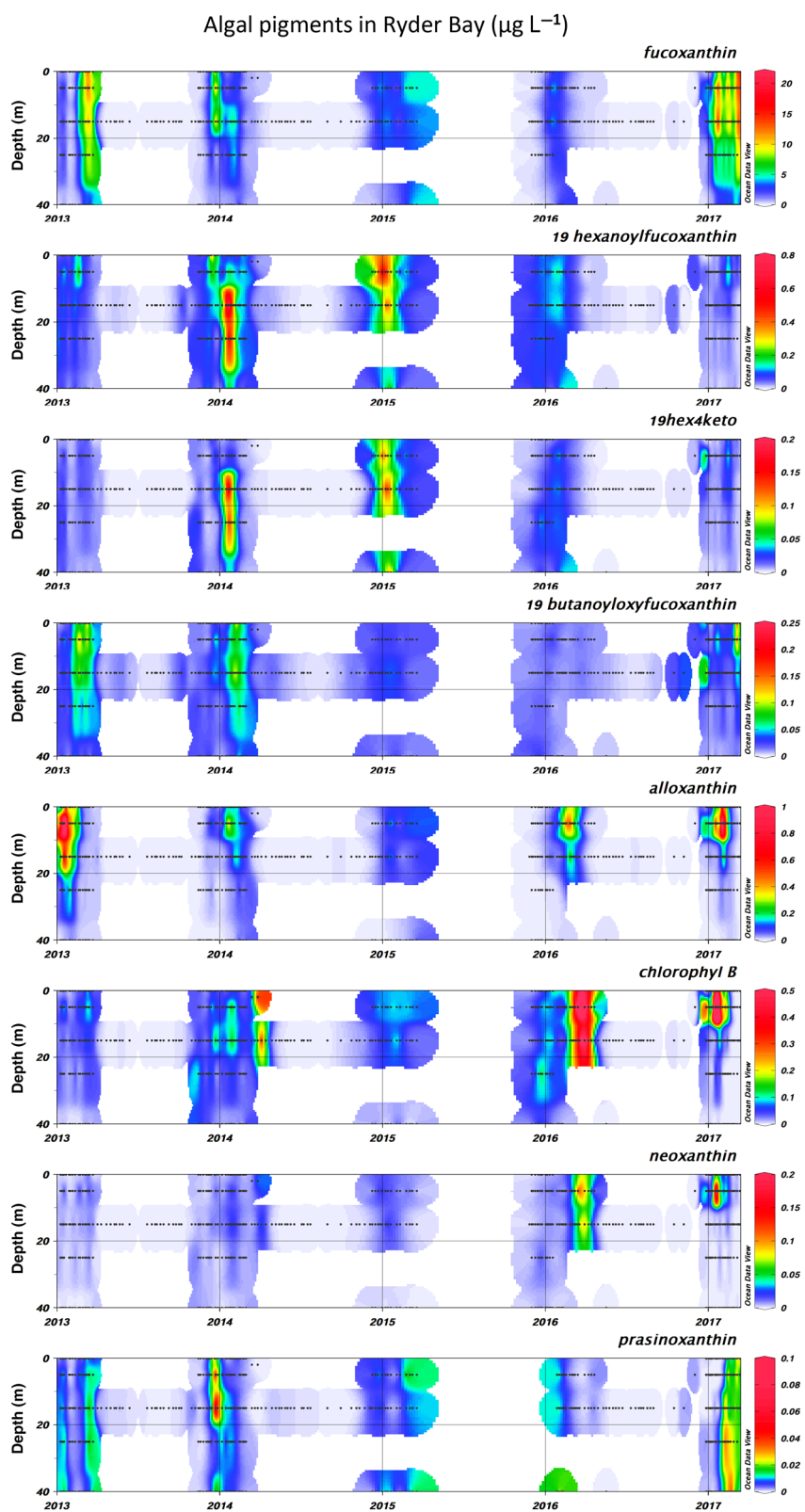


**Fig. 4.** Time series of algal pigments ( $\mu\text{g L}^{-1}$ ). No samples were taken in the winters of 2014 and 2015.

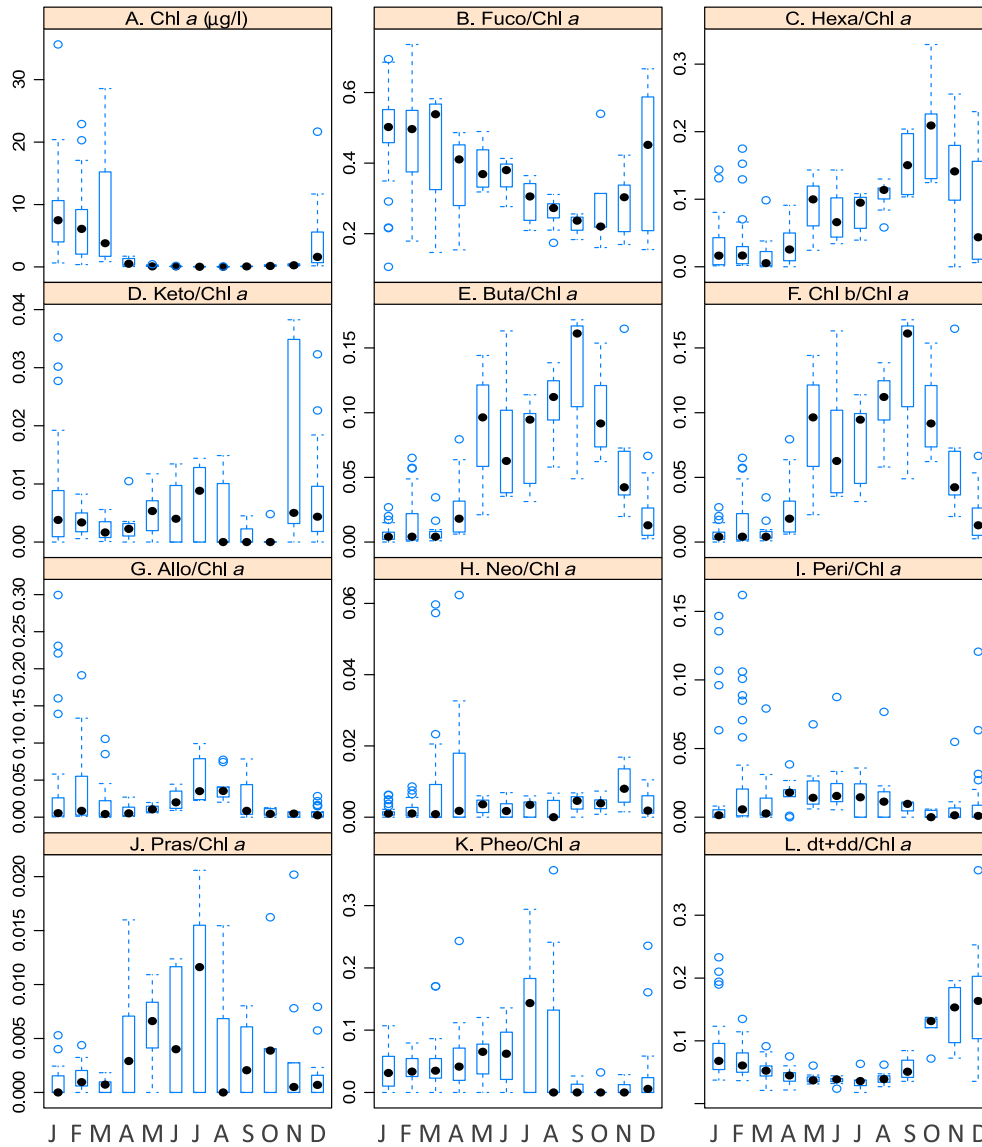


**Fig. 5.** Pigment patterns for samples taken at 15 m depth, as an average over all 5 years. Chl *a* is shown in  $\mu\text{g L}^{-1}$ . All other panels show ratios of pigment per Chl *a* (Chl *a* as determined by HPLC). Zeros scores for dt/dt + dd in winter (months 5–9) resulted from values of dt that are below detection limit. Circles represent outliers. For all abbreviations see text.

gradually decreased towards winter, and rapidly picked up again from October–November onwards (Fig. 5).

Species succession between November and March was also very distinct when all summer pigment data were pooled together and analyzed with Chemtax (Fig. 6). Autotrophic flagellates (Haptophytes\_P and C, chlorophytes, and prasinophytes) were dominant in spring and gradually dropped towards January. Prominent species identified by microscopy were *Chrysochromulina* sp., *Micromonas* sp., *Pyramimonas* spp., and single celled *P. antarctica* (Table 3). Whereas high numbers of *Chaetoceros* sp. were observed in spring 2013, diatoms were overall most abundant from January to March (Fig. 6). In January–February, smaller

centrics like *Thalassiosira* sp. ( $< 20 \mu\text{m}$ ) were more abundant, but large centric species like *Proboscia inermis* and *Corethron* sp. probably contributed mostly to biovolume. (Table 3). High numbers of small cryptophytes (5–20  $\mu\text{m}$ ) were also observed in January. Dinoflagellates were only present in very low abundances, though microscopy showed that species like *Gymnodinium* sp. and *Prorocentrum* were almost always present.

#### Photophysiology

In general, the algal communities were healthy, with maximum yield values  $\sim 0.7$ – $0.8$  (Fig. 7a,b). The lowest values for Fv/Fm were recorded early summer in surface waters; high

**Table 3.** The dominant algal species determined by microscopy in samples taken in January and February 2013 and in the summer season of 2013/2104. Algal abundance is presented as percentage of total cell numbers. The species listed include 50%–70% of total cell numbers. Unidentified flagellates account for the majority of the remaining cells.

Class	Species	Jan–Feb 2013	Nov–Dec 2013	Jan–Feb 2014	
Bacillariophyceae (diatoms)	<i>Amphiprora kufferathii</i>	<1	<1	<1	
	<i>Biddulphia aurita</i>	<1	0	<1	
	<i>Chaetoceros</i> sp. (10–15 $\mu\text{m}$ ) <sup>a</sup>	3	40	5	
	<i>Cocconeis fasciolata</i>	<1	<1	0	
	<i>Corethron</i> sp.	<1	4	<1	
	<i>Coscinodiscus bouvet</i>	<1	0	<1	
	<i>Eucampia antarctica</i>	<1	<1	<1	
	<i>Fragilariopsis cylindrus/curta/</i> <i>keruelensis</i> /sp.	<1	<1	5	
	<i>Navicula</i> sp.	0	<1	<1	
	<i>Nitzschia</i> spp.	<1	4	5	
	<i>N. longissima</i> / <i>C. closterium</i>	0	<1	<1	
	<i>Proboscia inermis/truncata</i>	<1	<1	<1	
	<i>Pseudo-nitzschia</i>	4	<1	<1	
	<i>Thalassiosira</i> sp. (5–20 $\mu\text{m}$ ) <sup>a</sup>	23	<1	0	
	<i>Trichotoxon reinboldii</i>	0	<1	2	
	Prymnesiophyceae (Haptophyceae)	<i>Phaeocystis antarctica</i>	4	5	16
		<i>Chrysochromulina</i> sp.	2	13	4
Prasinophyceae	<i>Pyramimonas</i> sp.	<1	1	3	
	<i>Micromonas</i> sp.	0	1	<1	
Cryptophyceae	<i>Cryptophyte</i> sp.	13	3	19	
Dinophyceae (dinoflagellates)	<i>Amphidinium sphenoides</i>	<1	<1	<1	
	<i>Gymnodinium cf. ostenfeldii</i>	0	1	1	
	<i>Gymnodinium</i> / <i>Gyrodinium</i> sp.	0	1	1	
	<i>Gymnodinium</i> sp.	3	1	3	
	<i>Gyrodinium cf. lachryma/spirale</i>	0	<1	<1	
	<i>Heterocapsa cf. triquetra</i>	<1	<1	<1	
	<i>Karenia</i> sp.	0	<1	1	
	<i>Katodinium glaucum</i>	<1	<1	<1	
	<i>Peridioides</i>	<1	<1	1	
	<i>Polarella glacialis</i>	0	<1	<1	
	<i>Prorocentrum</i>	<1	<1	<1	
	<i>Protoperdinium</i>	<1	0	<1	
	<i>Scropsiella/Peridiniella</i> sp.	0	<1	<1	

<sup>a</sup>Cell length.

values were recorded in deeper waters (Fig. 7a). The pattern was most clear in the season of 2016–2017, but was representative for all summer seasons ( $p < 0.05$ ). Likewise,  $\alpha$  displayed seasonality (Fig. 7d), with low values in the surface and maxima in deeper waters (Fig. 7c). The effective yield averaged between 0.3 and 0.5, with minimum values in January (Table 2). Rapid recovery after induction ( $IC_{\text{Rec}}$ ) was observed, with again minimum values in January (Table 2).

After light shock treatment, Fv/Fm dropped severely, sometimes to zero (Fig. 8). Recovery of Fv/Fm under dim light resulted in full recovery for surface communities. Communities sampled at 15 m and below suffered photoinhibition, as

reflected in poor recovery in January and February (Fig. 8; Table 2). Recovery ( $K_m$ ) in November and December was almost instantaneous; recovery in January and February took significantly longer (Table 2).

## Discussion

Algal dynamics at the WAP display seasonal and interannual fluctuations in relation to variations in environmental conditions. The strongest perturbation witnessed between 2012 and 2017 in Ryder Bay coincided with the El Niño that started in December 2015 and that had a strong impact on incident

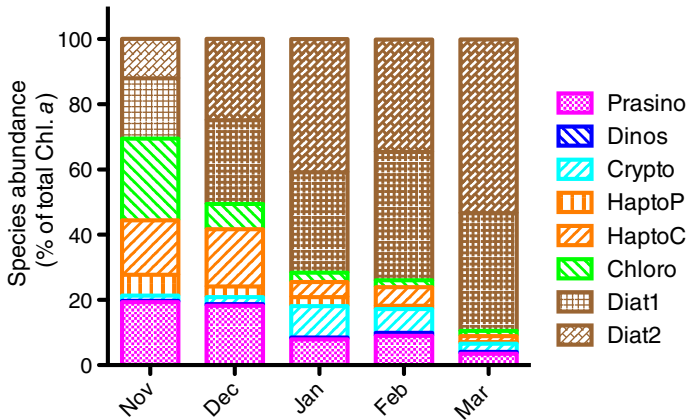


**Fig. 6.** Algal classes derived by Chemtax analyses, presented as a percentage of total Chl *a* (average values for all depths over all five summer seasons November–March).

irradiance and sea-ice cover. Despite the presence of such inter-annual variability, the data used here is sufficiently long for unequivocal seasonal patterns in species succession and driving mechanisms to be established. The photophysiological studies presented here add the essential details to previously established more general patterns (a.o. Rozema et al. 2017a; Schofield et al. 2017) that were required to elucidate the mechanisms that drive algal phenology. Our paper shows that photophysiological characteristics allow algal species to adapt to changing environmental conditions that may come along with climate change. Based on these findings and building on the outcome of recent models (e.g. Moreau et al. 2015), as will

be argued below, we predict sustained high algal production in Antarctic coastal areas, for the near-future.

### Algal phenology and environmental drivers

A composition of pigment data collected over five consecutive years clearly revealed that the onset of algal growth in spring started with mostly flagellate species (Fig. 5). The phenology of algal classes was reflected in a CCA diagram, in which the algal communities in Ryder Bay were organized according to their pigment composition in relation to their environmental drivers (Fig. 9; see Table 4 for statistics). Communities that shape the onset of algal blooms with the break-up of sea ice were most closely related to low-density surface waters modulated by low-salinity input and a deep MLD (Fig. 9; November–December). In transition towards summer (Fig. 9; Jan–March), algal communities developed that are mostly driven by light availability (SRD) and temperature. The autumn communities in March–July again formed a separate group that sustained the decreases in SRD and temperature. Winter communities (Fig. 9; July–October) formed groups associated with the full ranges of meteoric water, which is enigmatic. A strong association with cold waters and a shallow MLD indicates that winter communities were trapped in surface meltwater lenses.

The transition of the various algal communities carrying specific algal classes is thus clearly driven by environmental factors that dominate the Antarctic ecosystem: sea ice, temperature and light availability as defined in the CCA by density and SRD. The spring communities that related most closely with low density surface water in early spring are marked by

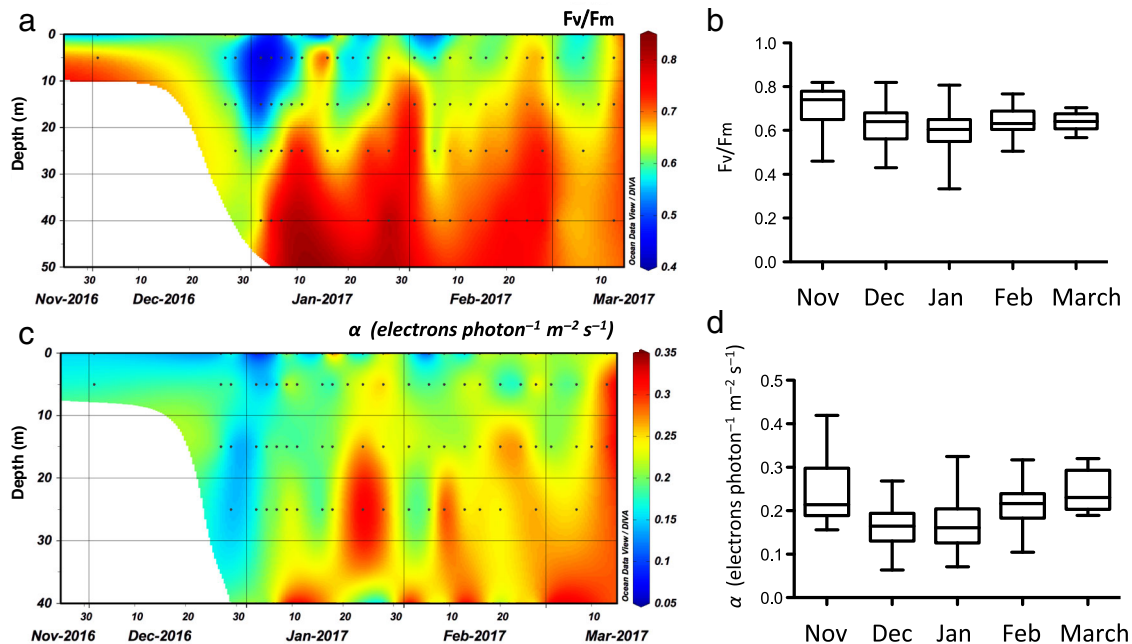


**Fig. 7.** Seasonal patterns in photophysiology (1) as a full profile over the summer season of 2016/2017 plotted as an example for  $F_v/F_m$  (a) and  $\alpha$  (c) and (2) as 5-year averages pooling data from all depths, of  $F_v/F_m$  (b) and  $\alpha$  (d)

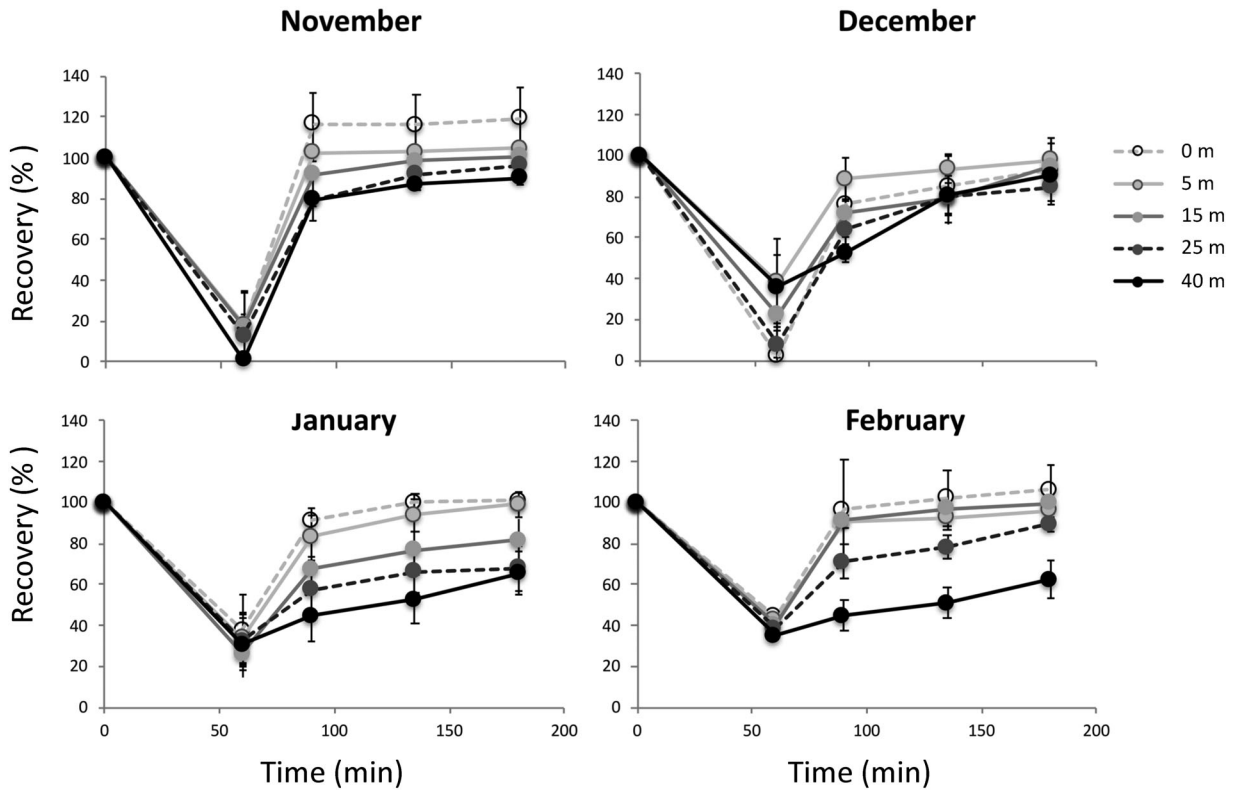


**Fig. 8.** Recovery of Fv/Fm after exposure to excessive light for 60 min, displayed for the four consecutive summer months (averages values over five summer seasons,  $\pm$  SD).

Hexa, fingerprinting haptophytes. Fuco linked to the development of diatom blooms later in the season, which are most

dependent on increased SRD and higher temperatures. The sub-surface bloom of haptophytes in summer 2014 (Fig. 4) was linked to a prolonged period of strong wind and a rapid deepening of the MLD (data not shown). The summer transition from Hexa to Fuco-containing species is marked by Allo, signaling the presence of cryptophyte algae that seem to occupy the space when no other classes are present. Small flagellate species containing Chl *b* are omnipresent as background communities in low concentrations and most resilient in winter.

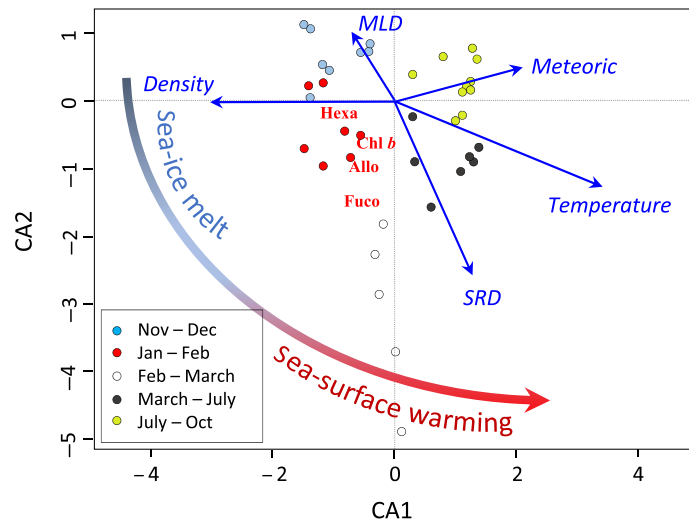


**Fig. 9.** Ordination plot of a CCA analysis of marker pigments and abiotic parameters (blue arrows) collected over five years at 15 m depth, plotted as monthly averages. To avoid extreme forcing by outliers, data collected at 40 m were excluded from the analyses. The first two axes explain 94% of the variance. All vectors in togetherness are highly significant (ANOVA;  $p < 0.001$ ).

Sea ice was identified as an important component in driving algal growth and defining the community composition. The link between sea-ice and pelagic communities is somewhat enigmatic. Sea-ice algae may form an important component of pelagic communities but it is also frequently found that sea-ice algae are no longer vital once released in the water column (Arrigo 2014; van Leeuwe et al. 2018). Mesocosm experiments near the marginal ice zone (MIZ) of the southern Atlantic did confirm that the seeding potential of sea ice in synergy with stratification induced by ice melt provides good conditions for algal blooms (Giesenhagen et al. 1999). Studies in the WAP region also associated elevated algal biomass with the presence of sea ice (Vernet et al. 2008; Arrigo et al. 2017; Selz et al. 2018). Our data in Ryder Bay again reveal a direct connection between the sea ice and the pelagic system. The

**Table 4.** Significance levels of specific environmental parameters for individual pigments derived by linear modeling (Chl *a* was tested as a function of temperature, salinity and MLD; the other pigments as a function of all parameters except salinity). n.s., not significant; n.d., not determined; for abbreviations, see text.

	Temperature	Salinity	MLD	Density	SRD	Meteo
Chl <i>a</i>	<0.0005	<0.0005	<0.05	n.s.	n.s.	n.s.
Hexa	n.s.	n.s.	n.s.	<0.0005	<0.0005	<0.0005
Fuco	<0.005	n.s.	<0.005	<0.005	n.s.	n.s.
Allo	<0.0005	n.s.	n.s.	n.s.	n.s.	<0.05
Chl <i>b</i>	n.s.	n.s.	n.s.	<0.005	n.s.	n.s.

presence in the seawater of ice-dwelling species like *Pyramimonas* sp. (Prasinophyceae) and the dinoflagellate *Polarella glacialis*, strongly suggested that sea ice acted as a seeding vector for the pelagic. The temporal study in Ryder Bay matched a regional survey extending over the shelf that also indicated strong linkages between sea-ice melt and haptophyte microalgal abundance in surface waters (Stefels et al. 2018).

#### Algal phenology and photophysiological characteristics

The variable light conditions, over the year as well as within the summer season, require flexible photosynthetic responses by algae. Clear patterns of photoacclimation were observed over the summer season, complementary to trends in environmental drivers. The seasonal patterns in photophysiological characteristics could again be connected to the succession of algal classes (Fig. 10). The spring community in November/December, dominated by autotrophic flagellates, had a strong association with a high affinity for light ( $\alpha$ ) and high photosynthetic activity ( $P_{max}$ ). In summer (Fig. 10; January), the diatom communities were characterized by longer recovery duration,  $K_m$ , and to a lesser extent  $IC_{Rec}$ .

These patterns follow predicted species-specific photophysiological responses. In general, flagellates have a higher photoflexibility compared to diatoms, related to a more flexible make-up of photosynthetic membranes in green algae (Richardson et al. 1983; van Leeuwe et al. 2005). Summer minima in Fv/Fm and  $\alpha$ , associated with higher contributions of the xanthophyll pool in December and January (Fig. 5;  $dt + dd/Chl a$ ), reflected down-regulation of photosynthetic activity to avoid photoinhibition (Alderkamp et al. 2013; Smith et al. 2013). Whereas both diatoms and haptophytes like *P. antarctica* display very effective xanthophyll cycling (van Leeuwe and Stefels 2007; Alderkamp et al. 2010), diatoms experience growth reduction under dynamic light conditions due to metabolic deficiencies (Kropuenske et al. 2010). Likewise, experiments showed higher photophysiological flexibility in the prasinophyte *Pyramimonas* sp. compared to the diatom *Chaetoceros brevis* (van Leeuwe et al. 2005).

The cryptophyte communities in January/February stand out clearly (Fig. 10). The occurrence of cryptophytes in summer confirms that they can cope well with high light conditions by very effective xanthophyll cycling (Russo et al. 2018). Yet

cryptophytes had a negative relationship to photophysiological parameters in the CCA analyses (Fig. 10). The real success of cryptophytes may relate to a mixotrophic life style. Mixotrophy may be far more common in polar regions than so far acknowledged (Stoecker and Lavrentyev 2018). Notably, in winter elevated levels of Allo/Chl *a* - marking cryptophytes - coincided with the winter peak in pheophorbide (Fig. 5), a pigment that is a breakdown product of Chl *a* and associated with grazing (Louda et al. 2011). Mixotrophy would also explain their appearance often following algal blooms (this study, Garibotti et al. 2005; Goldman et al. 2015), when concentrations of dissolved organic compounds are often high. It also explains the contradictory findings regarding their preference for high temperatures in Bransfield Strait (Rodriguez et al. 2002; Moline et al. 2004) versus low temperatures near Palmer Station (Schofield et al. 2017). The common denominator in these waters is their confinement to shallow layers, which may be associated with a relatively low (micro-) nutrient supply.

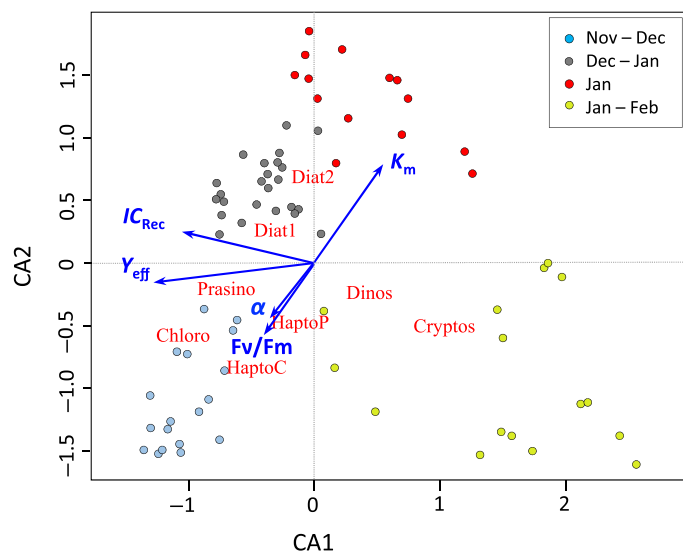


**Fig. 10.** Ordination plot of a CCA analysis of species composition and photophysiological parameters (blue arrows) collected over five years. The first two axes explain 58% of the variance. All vectors in together are significant (ANOVA;  $p < 0.05$ ).

### Inter-annual variation

On interannual timescales, variations in community structure occurred that can be linked to established environmental drivers. Overall, the algal community dynamics observed were typical for Ryder Bay (Annett et al. 2010; Rozema et al. 2017a, b). Chl *a* concentration in algal blooms varied between 10 and 40  $\mu\text{g L}^{-1}$ , representative of coastal waters of the WAP (Vernet et al. 2008; Kim et al. 2018). Between 2013 and 2017, in four out of 5 years two consecutive blooms were observed, in accord with previously described patterns (Clarke et al. 2008; Annett et al. 2010). Over the five years sampled, the best predictors for Chl *a* were environmental parameters that related to sea-ice melt, which explained the spring blooms, and stratification (Table 4: salinity, temperature, and MLD, respectively). A shallow summer MLD correlated with the high chlorophyll years in 2013 and 2017.

The intermediate years of 2014–2016 were years of low biomass, and as such did not corroborate with established connections that link winters with strong sea-ice cover to successive summers with high chlorophyll biomass (Venables et al. 2013). The interannual variation stipulate the influence of local oceanographic conditions on growth control. In the summer of 2013/2014, algal growth was suppressed by deep wind mixing preventing the build-up of biomass (Rozema et al. 2017b). This season was characterized by the dominance of flagellate species, marked by high Hexa concentrations (Fig. 4). The summer of 2014/2015 was highly dynamic; ice conditions in Ryder Bay varied on almost a daily basis (pers. obs.). Periodic ice melt likely resulted in pulsed seeding events of algal communities, as indicated by the presence of flagellate species. Chl *a* concentrations

were relatively low in terms of biomass but of significant importance for ecosystem dynamics: the fluxes of organic sulfur compounds (dimethyl sulfide) associated with the micro-algal communities were the highest over the full period of observations between 2012 and 2017 (Webb et al. 2019).

The importance of sea ice as vector for algal biomass was once more confirmed by the record in Chl *a* concentration observed in the post-El Niño season of 2016/2017. The 2015/2016 El Niño event coupled to a negative phase of the Southern Annular Mode (SAM) resulted in low incident irradiance during summer. The sub-optimal light climate favored non-haptophyte flagellate species. This summer was followed by a record Antarctic sea-ice retreat in spring 2016/2017, but conversely an extremely late sea-ice retreat in Ryder Bay possibly related to atmospheric anomalies associated with changes in wind patterns (Turner et al. 2017). Consequently, in 2016 sea ice remained until end of December, which resulted in a delayed spring bloom that only occurred end of January 2017. The rapid break-up of the ice-sheet not only triggered a diatom bloom, but seeding by ice-algae seemed also to affect the algal community. Chl *b* and Neo were anomalously high, indicating the presence of flagellate species. Unfortunately, no microscopic data are available to identify the species composition.

### Ecology of Antarctic coastal zones under climate change: future predictions

The five-year time series showed that algal growth in the WAP is subject to atmospheric and oceanographic forcings, and thereby susceptible to climate change. During the second

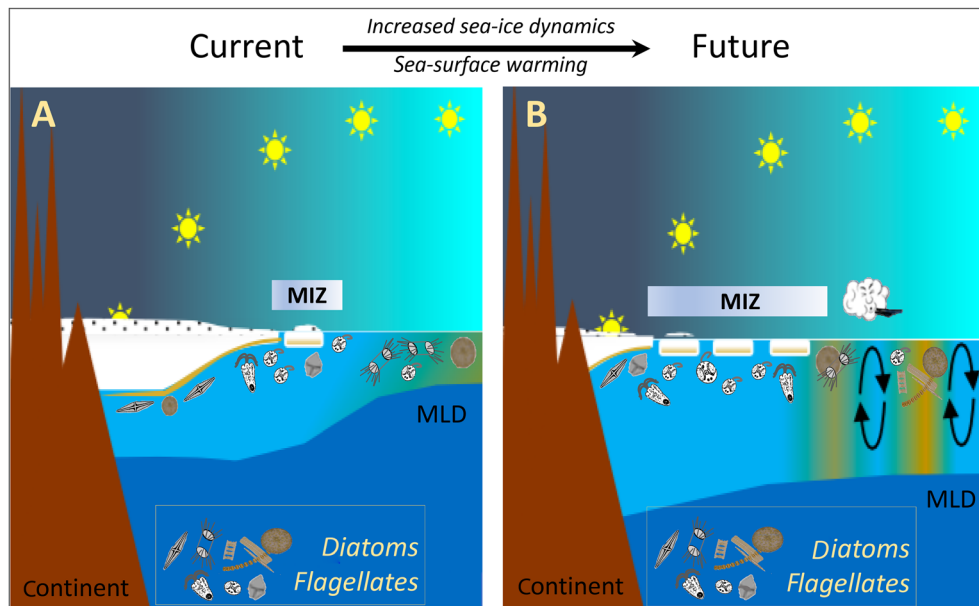


**Fig. 11.** Algal community structure in the WAP linked to sea-ice conditions, depicting two dominant groups. **(a)** Current conditions in which high biomass in spring is associated with flagellates and summer blooms are dominated by diatoms. **(b)** Future conditions with more dynamic ice cover hosting larger flagellate communities and more dispersed summer blooms controlled by wind mixing. Primary production and algal biomass (indicated as brown shades) is predicted to increase in the near future.

half of the twentieth century, atmospheric temperatures at the WAP rose most rapidly of any region in the Southern Hemisphere, and surface ocean temperatures increased concomitantly by over 1°C (Meredith and King 2005). Sea ice retreated rapidly since the start of the satellite era, with the sea-ice season decreasing by 85 days (Stammerjohn et al. 2008). Increased upwelling of warm UCDW onto the shelf was also evidenced, strengthening the supply of heat and macronutrients to the shelf waters (Moffat and Meredith 2018). Since the turn of the century, atmospheric temperatures have stabilized and even cooled along the WAP (Turner et al. 2016), though this is currently interpreted as the imprint of natural inter-annual variability, and the long-term warming trend is thus expected to resume albeit at a time not yet known. The combination of large-scale forcings (a.o. SAM, El Niño Southern Oscillation (ENSO), atmospheric warming) and local forcings responsible for these trends and current reversals has not been unambiguously established, however the sensitivity of the WAP to climatic variability is clear (Henley et al. 2019).

The consequences of ongoing ice retreat for algal communities are not unequivocal due to the complexity of the relationship between sea-ice cover and algal production. Available model predictions cover very large scales (Earth System Models as reviewed by Henson et al. 2016) and regional scale modeling on impact of climate change requires decades of data to become reliable. Yet, there are indications for an increase in production in the Southern Ocean (Henson et al. 2016) and we also foresee a positive signal for the WAP within the near-future. Production at the coastal WAP and the wider Antarctic MIZ will become more variable in space and time. Under the presumption that sea ice will not fully disappear, the MIZ will always be a place of enhanced primary production (Lancelot et al. 1991; Ducklow et al. 2012; Arrigo 2014; Deppeler and Davidson 2017). The melting sea-ice acts as seeding vector (van Leeuwe et al. 2018), it may carry high nutrient loads (Fripiat et al. 2017) and provides shelter against grazing (Arrigo 2014). The importance of sea ice was well illustrated in Ryder Bay; the first algal bloom that was associated with sea-ice melt was the most regular feature in terms of algal biomass. With ongoing climate change sea ice will become more dynamic, including more episodic melt events and therewith an increased potential for biological activity at the MIZ. Flagellate species like haptophytes (e.g. *P. antarctica*), prasinophytes (e.g. *Pyramimonas* sp.) and chlorophytes will benefit from these developments and increase in numbers (Fig. 11). This is in fact already observed in coastal waters of the WAP where *Phaeocystis* occupies areas of dynamic ice cover (Arrigo et al. 2017; Stefels et al. 2018).

Away from the optimal habitat that is provided by the MIZ, algal blooms most likely will become less in magnitude but more widespread. Increasing wind speeds that are associated with a positive SAM will have negative effects on water column stratification. Besides our study in Ryder Bay, previous studies at the western WAP already showed that an unstable

water column prevents the development of large diatom blooms (Schofield et al. 2017; Rozema et al. 2017a). However, additional studies in the northern WAP (Schloss et al. 2012) and over the western WAP-shelf area (Montes-Hugo et al. 2009; Schofield et al. 2017; Kim et al. 2018; Henley et al. 2019) showed that local conditions like local currents and wind patterns have an overriding impact on algal growth, opposing large-scale forcings. Whereas the local discrepancies seem to hinder future-forecasting, general patterns are becoming apparent. With the opening up of ice sheets, light availability will increase and the productive season for algal growth extended (Fig. 11). Taking regional and temporal decline into account (e.g. like observed by Montes-Hugo et al. 2009), current studies in the northwestern WAP already showed that primary production has increased by roughly 30% since the beginning of this century (Smith and Comiso 2008; Moreau et al. 2015). These results may furthermore be explained by faster production and turnover rates in surface waters that may be connected to increasing temperatures. Besides our observations, a number of laboratory and field studies have shown that especially diatoms seem to profit from increasing temperatures (Xu et al. 2014; Zhu et al. 2016, 2017), unlike species like *P. antarctica* that have a rather low temperature preference (< 4°C). Enhanced bloom dynamics will also favor cryptophyte species. Presuming that they are indeed mixotrophic, cryptophytes will benefit from decaying blooms. By being dependent on the general trends in biomass development cryptophytes are, however, unlikely to become dominant players.

## References

- Alderkamp, A. C., H. W. J. De Baar, R. J. W. Visser, and K. R. Arrigo. 2010. Can photoinhibition control phytoplankton abundance in deeply mixed water columns of the Southern Ocean? *Limnol. Oceanogr.* **55**: 124821264. doi:10.4319/lo.2010.55.3.1248
- Alderkamp, A. C., M. M. Mills, G. L. van Dijken, and K. R. Arrigo. 2013. Photoacclimation and non-photochemical quenching under in situ irradiance in natural phytoplankton assemblages from the Amundsen Sea, Antarctica. *Mar. Ecol. Prog. Ser.* **475**: 15234. doi:10.3354/meps10097
- Annett, A. L., D. S. Carson, X. Crosta, A. Clarke, and R. S. Ganeshram. 2010. Seasonal progression of diatom assemblages in surface waters of Ryder Bay, Antarctica. *Polar Biol.* **33**: 13–29. doi:10.1007/s00300-009-0681-7
- Annett, A. L., S. F. Henley, H. J. Venables, M. P. Meredith, A. Clarke, and R. S. Ganeshram. 2017. Silica cycling and isotopic composition in northern Marguerite Bay on the rapidly-warming western Antarctic Peninsula. *Deep. Res. Part II Top. Stud. Oceanogr.* **139**: 132–142. doi:10.1016/j.dsr2.2016.09.006
- Arrigo, K. R. 2014. Sea ice ecosystems. *Ann. Rev. Mar. Sci.* **6**: 439–467.

- Arrigo, K. R., D. H. Robinson, D. L. Worthen, R. B. Dunbar, G. R. DiTullio, M. VanWoert, and M. P. Lizotte. 1999. Phytoplankton community structure and the drawdown of nutrients and CO<sub>2</sub> in the Southern Ocean. *Science* **283**: 365–367. doi:[10.1126/science.283.5400.365](https://doi.org/10.1126/science.283.5400.365)
- Arrigo, K. R., G. L. van Dijken, A. C. Alderkamp, Z. K. Erikson, K. M. Lewis, K. E. Lowry, H. L. Joy-Warren, R. Middag, et al. 2017. Early spring phytoplankton dynamics in the western Antarctic Peninsula. *J. Geophys. Res. - Ocean.* **122**: 9350–9368.
- Bown, J., H. Van Haren, M. P. Meredith, H. J. Venables, P. Laan, J. A. Brearley, and H. J. W. de Baar. 2018. Evidence of strong sources of DFe and DMn in Ryder Bay, Western Antarctic Peninsula. *Philos. Trans. R. Soc. A* **376**. doi:[10.1098/rsta.2017.0172](https://doi.org/10.1098/rsta.2017.0172)
- Clarke, A., M. P. Meredith, M. I. Wallace, M. A. Brandon, and D. N. Thomas. 2008. Seasonal and interannual variability in temperature, chlorophyll and macronutrients in northern Marguerite Bay, Antarctica. *Deep. Res. Part II Top. Stud. Oceanogr.* **55**: 1988–2006. doi:[10.1016/j.dsr2.2008.04.035](https://doi.org/10.1016/j.dsr2.2008.04.035)
- Deppeler, S. L., and A. T. Davidson. 2017. Southern Ocean phytoplankton in a changing climate. *Front. Mar. Sci.* **4**: 40.
- Ducklow, H. W., A. Clarke, R. Dickhut, S. C. Doney, H. Geisz, K. Huang, D. G. Martinson, M. P. Meredith, and others. 2012. The marine system of the Western Antarctic Peninsula, p. 121–159. *In* A. D. Rogers, N. M. Johnston, E. J. Murphy, and A. Clarke [eds.], *Antarctic Ecosystems*. Chichester, United Kingdom: John Wiley and Sons, Ltd..
- Fripiat, F., K. M. Meiners, M. Vancoppenolle, S. Papadimitriou, D. N. Thomas, S. F. Ackley, K. R. Arrigo, G. Carnat, and others. 2017. Macro-nutrient concentrations in Antarctic pack ice: Overall patterns and overlooked processes. *Elem. Sci. Anth.* **5**: 13. doi:[10.1525/elementa.217](https://doi.org/10.1525/elementa.217)
- Garibotti, I. A., M. Vernet, and M. Ferrario. 2005. Annually recurrent phytoplanktonic assemblages during summer in the seasonal ice zone west of the Antarctic Peninsula (Southern Ocean). *Deep. Res. Part I Oceanogr. Res. Pap.* **52**: 1823–1841.
- Giesenhausen, H. C., A. E. Detmer, J. de Wall, A. Weber, R. R. Gradinger, and F. J. Jochem. 1999. How are Antarctic planktonic microbial food webs and algal blooms affected by melting of sea ice? Microcosm simulations. *Aquat. Microb. Ecol.* **20**: 183–201.
- Goldman, J. A. L., S. A. Kranz, J. N. Young, P. D. Tortell, R. H. R. Stanley, M. L. Bender, and F. M. M. Morel. 2015. Gross and net production during the spring bloom along the Western Antarctic Peninsula. *New Phytol.* **205**: 182–191.
- Grasshoff, K. 1983. Determination of nutrients, p. 143–150. *In* K. Grasshoff, M. Ehrhardt, and M. Kremling [eds.], *Methods of seawater analysis*. Weinheim: Verlag Chemie.
- Henley, S. F., O. M. Schofield, K. R. Hendry, I. R. Schloss, D. K. Steinberg, C. Moffat, L. S. Peck, D. P. Costa, and others. 2019. Variability and change in the west Antarctic Peninsula marine system: Research priorities and opportunities. *Progr. Oceanogr.* **173**: 208–237.
- Henson, S. A., C. Banlieu, and R. Lampitt. 2016. Observing climate change trends in ocean biogeochemistry: When and where. *Glob. Change Biol.* **22**: 1561–1571.
- Hughes, C., A. L. Chuck, H. Rossetti, P. J. Mann, S. M. Turner, A. Clarke, R. Chance, and P. S. Liss. 2009. Seasonal cycle of seawater bromoform and dibromomethane concentrations in a coastal bay on the western Antarctic Peninsula. *Global Biogeochem. Cycles* **23**: GB2024. doi:[10.1029/2008GB003268](https://doi.org/10.1029/2008GB003268)
- Kim, H., and others. 2018. Interdecadal variability of phytoplankton biomass accumulation along the coastal West Antarctic Peninsula. *Philos. Trans. R. Soc. A* **376**: 20170174.
- Kropuenske, L. R., M. M. Mills, G. L. Van Dijken, A. C. Alderkamp, G. M. Berg, D. H. Robinson, N. A. Welschmeyer, and K. R. Arrigo. 2010. Strategies and rates of photoacclimation in two major Southern Ocean phytoplankton taxa: *Phaeocystis antarctica* (haptophyta) and *Fragilariopsis cylindrus* (bacillariophyceae). *J. Phycol.* **46**: 1138–1151.
- Lancelot, C., G. Billen, C. Veth, S. Becquevort, and S. Mathot. 1991. Modelling carbon cycling through phytoplankton and microbes in the Scotia-Weddell Sea area during sea ice retreat. *Mar. Chem.* **35**: 305–324.
- Legge, O. J., D. C. E. Bakker, M. P. Meredith, H. J. Venables, and P. J. Brown. 2017. The seasonal cycle of carbonate system processes in Ryder Bay, West Antarctic Peninsula. *Deep. Res. Part II Top. Stud. Oceanogr.* **39**: 167–180. doi:[10.1016/j.dsr2.2016.11.006](https://doi.org/10.1016/j.dsr2.2016.11.006)
- Liu, X., and W. O. Smith. 2012. Physicochemical controls on phytoplankton distribution in the Ross Sea, Antarctica. *J. Mar. Syst.* **94**: 135–144.
- Louda, J. W., P. Mongkhonsri, and E. W. Baker. 2011. Chlorophyll degradation during senescence and death-III: 3-10 yr experiments, implications for ETIO series generation. *Org. Chem.* **42**: 688–699.
- Meijers, A. J. S. 2014. The Southern Ocean in the Coupled Model Intercomparison Project phase 5. *Philos. Trans. R. Soc.* **A372**: 20130296. doi:[10.1098/rsta.2013.0296](https://doi.org/10.1098/rsta.2013.0296)
- Mendes, C. R. B., V. M. Tavano, M. C. Leal, M. S. de Souza, V. Brotas, and C. A. E. Garcia. 2013. Shifts in the dominance between diatoms and cryptophytes during three late summers in the Bransfield Strait (Antarctic Peninsula). *Polar Biol.* **36**: 537–547. doi:[10.1007/s00300-012-1282-4](https://doi.org/10.1007/s00300-012-1282-4)
- Meredith, M. P., and C. J. King. 2005. Rapid climate change in the ocean west of the Antarctic Peninsula during the second half of the 20th century. *Geophys. Res. Lett.* **32**: 1–5. doi:[10.1029/2005GL024042](https://doi.org/10.1029/2005GL024042)
- Meredith, M. P., S. E. Stammerjohn, H. J. Venables, H. W. Ducklow, D. G. Martinson, R. A. Iannuzzi, M. J. Leng, J. M. van Wessem, and others. 2017. Changing distributions of sea ice melt and meteoric water west of the Antarctic Peninsula. *Deep. Res. Part II Top. Stud. Oceanogr.* **139**: 40–57. doi:[10.1016/j.dsr2.2016.04.019](https://doi.org/10.1016/j.dsr2.2016.04.019)

- Moffat, C., and M. Meredith. 2018. Shelf-ocean exchange and hydrography west of the Antarctic Peninsula: A review. *Philos. Trans. R. Soc.* **A376**: 20170164.
- Moline, M. A., H. Claustre, T. K. Frazer, O. Schofield, and M. Vernet. 2004. Alteration of the food web along the Antarctic Peninsula in response to a regional warming trend. *Glob. Change Biol.* **10**: 1973–1980. doi:[10.1111/j.1365](https://doi.org/10.1111/j.1365)
- Montes-Hugo, M., S. C. Doney, H. W. Ducklow, W. R. Fraser, D. Martinson, S. E. Stammerjohn, and O. Schofield. 2009. Recent changes in phytoplankton communities associated with rapid regional climate change along the western Antarctic Peninsula. *Science* **323**: 1470–1473. doi:[10.1126/science.1164533](https://doi.org/10.1126/science.1164533)
- Moreau, S., B. Mostajir, S. Belanger, I. Schloss, M. Vancoppenolle, S. Demers, G. Ferreyra, and G. 2015. Climate change enhances primary production in the western Antarctic Peninsula. *Glob. Change Biol.* **21**: 2191–2205.
- Olaizola, M., J. La Roche, Z. Kolber, and P. G. Falkowski. 1994. Non-photochemical fluorescence quenching and the diadinoxanthin cycle in a marine diatom. *Photosynth. Res.* **41**: 357–370.
- Platt, T. C., C. L. Gallegos, and W. G. Harrison. 1980. Photoinhibition of photosynthesis in natural assemblages of marine phytoplankton. *J. Mar. Res.* **38**: 687–701.
- Richardson, K., J. Beardall, and J. A. Raven. 1983. Adaptation of uni-cellular algae to irradiance: An analysis of strategies. *New Phytol.* **93**: 157–191.
- Rodriguez, F., F. Jimenez-Gomez, J. M. Blanco, and F. L. Figueroa. 2002. Physical gradients and spatial variability of the size and structure and composition of phytoplankton in the Gerlache Strait (Antarctica). *Deep. Res. Part II Top. Stud. Oceanogr.* **49**: 693–706.
- Rozema, P. D., G. Kulk, M. P. Veldhuis, A. G. J. Buma, M. P. Meredith, and W. H. van de Poll. 2017b. Assessing drivers of coastal primary production in Northern Marguerite Bay, Antarctica. *Front. Mar. Sci.* **4**: 184. doi:[10.3389/fmars.2017.00184](https://doi.org/10.3389/fmars.2017.00184)
- Rozema, P. D., H. J. Venables, W. H. van de Poll, A. Clarke, M. P. Meredith, and A. G. J. Buma. 2017a. Interannual variability in phytoplankton biomass and species composition in northern Marguerite Bay (West Antarctic Peninsula) is governed by both winter sea ice cover and summer stratification. *Limnol. Oceanogr.* **62**: 235–252. doi:[10.1002/lno.10391](https://doi.org/10.1002/lno.10391)
- Russo, A. D. A. P. G., M. Silva de Souza, C. R. B. Mendes, V. M. Tavano, and C. A. E. Garcia. 2018. Spatial variability of photophysiology and primary production rates of the phytoplankton communities across the western Antarctic Peninsula in late summer 2013. *Deep. Res. Part II Top. Stud. Oceanogr.* **149**: 99–110.
- Saba, G. K., W. R. Fraser, V. S. Saba, R. A. Iannuzzi, K. E. Coleman, S. C. Doney, H. W. Ducklow, D. G. Martinson, et al. 2014. Winter and spring controls on the summer food web of the coastal West Antarctic Peninsula. *Nat. Commun.* **5**: 4318. doi:[10.1038/ncomms5318](https://doi.org/10.1038/ncomms5318)
- Schloss, I. R., D. Abele, S. Moreau, S. Demers, A. V. Bers, O. Gonzalez, and G. A. Ferreyra. 2012. Response of phytoplankton dynamics to 19-year (1991–2009) climate trends in Potter Cove (Antarctica). *J. Mar. Syst.* **92**: 53–66.
- Schofield, O., G. Saba, K. Coleman, F. Carvalho, N. Couto, H. Ducklow, Z. Finkel, A. Irwin, and others. 2017. Decadal variability in coastal phytoplankton community composition in a changing West Antarctic Peninsula. *Deep. Res. Part I Oceanogr. Res. Pap.* **124**: 42–54.
- Selz, V., K. E. Lowry, K. M. Lewis, H. L. Joy-Warren, W. H. van de Poll, S. Nirmel, A. Tong, and K. R. Arrigo. 2018. Distribution of *Phaeocystis antarctica*-dominated sea ice algal communities and their potential to seed phytoplankton across the western Antarctic Peninsula in spring. *Mar. Ecol. Prog. Ser.* **586**: 91–112.
- Smith, W. O., and J. C. Comiso. 2008. The influence of sea ice on primary production in the Southern Ocean: A satellite perspective. *J. Geophys. Res.* **113**: C05S93. doi:[10.1029/2007JC004251](https://doi.org/10.1029/2007JC004251)
- Smith, W. O., S. Tozzi, M. C. Long, P. N. Sedwick, J. A. Peloquin, R. B. Dunbar, D. A. Hutchins, Z. Kolber, and G. R. DiTullio. 2013. Spatial and temporal variations in variable fluorescence in the Ross Sea (Antarctica): Oceanographic correlates and bloom dynamics. *Deep. Res. Part I Oceanogr. Res. Pap.* **79**: 141–155.
- Stammerjohn, S. E., D. G. Martinson, R. C. Smith, X. Yuan, and D. Rind. 2008. Trends in Antarctic annual sea ice retreat and advance and their relation to El Niño–Southern Oscillation and Southern Annular Mode variability. *J. Geophys. Res.* **113**: 1–20. doi:[10.1029/2007JC004269](https://doi.org/10.1029/2007JC004269)
- Stefels, J., M. A. van Leeuwe, and M. P. Meredith. 2017. Marine studies at the Western Antarctic Peninsula: Priorities, progress and prognosis. *Deep. Res. Part II Top. Stud. Oceanogr.* **139**: 1–8.
- Stefels, J., M. A. van Leeuwe, E. J. Jones, M. P. Meredith, H. J. Venables, A. L. Webb, and S. F. Henley. 2018. Impact of sea-ice melt on DMS(P) inventories in surface waters of Marguerite Bay, West Antarctic Peninsula. *Philos. Trans. R. Soc.* **A376**: 20170169.
- Steiner, N., and J. Stefels. 2017. Commentary on the outputs and future of Biogeochemical Exchange Processes at Sea-Ice Interfaces (BEPSII). *Elem. Sci. Anth.* **5**: 81. doi:[10.1525/elementa.272](https://doi.org/10.1525/elementa.272)
- Stoecker, D. K., and P. J. Lavrentyev. 2018. Mixotrophic plankton in the polar seas: A pan-Arctic review. *Front. Mar. Sci.* **5**: 292. doi:[10.3389/fmars.2018.00292](https://doi.org/10.3389/fmars.2018.00292)
- Turner, J., H. Lu, I. White, J. C. King, T. Phillips, J. S. Hosking, T. J. Bracegirdle, G. J. Marshall, and others. 2016. Absence of 21<sup>st</sup> century warming on Antarctic Peninsula consistent with natural variability. *Nature* **535**: 411–415.
- Turner, J., T. Phillips, G. J. Marshall, J. S. Hosking, J. O. Pope, T. J. Bracegirdle, and P. Deb. 2017. Unprecedented spring-time retreat of Antarctic sea ice in 2016. *Geophys. Res. Lett.* **44**: 6868–6875.
- Utermohl, H. 1958. Zur Vervollkommung der quantitativen Phytoplankton-Methodik. *Mitteilungen der Internationalen Verhandlung der Limnologie* **9**: 1–38.

- Vallina, S. M., and R. Simo. 2007. Strong relationship between DMS and the solar radiation dose over the global surface ocean. *Science* **315**: 506–508.
- van Heukelem, L., and C. S. Thomas. 2001. Computer-assisted high-performance liquid chromatography method development with applications to the isolation and analysis of phytoplankton pigments. *J. Chromatogr. A* **910**: 31–49. doi:10.1016/S0378-4347(00)00603-4
- van Leeuwe, M. A., G. Kattner, T. Van Oijen, J. T. M. de Jong, and H. J. W. de Baar. 2015. Phytoplankton and pigment patterns across frontal zones in the Atlantic sector of the Southern Ocean. *Mar. Chem.* **177**: 510–517.
- van Leeuwe, M. A., B. Van Sikkelerus, W. W. C. Gieskes, and J. Stefels. 2005. Taxon specific differences in photoacclimation to fluctuating irradiance in an Antarctic diatom and a green flagellate. *Mar. Ecol. Prog. Ser.* **288**: 9–19.
- van Leeuwe, M. A., L. A. Villerius, J. Roggeveld, R. J. W. Visser, and J. Stefels. 2006. An optimized method for automated analysis of algal pigments by HPLC. *Mar. Chem.* **102**: 267–275.
- van Leeuwe, M. A., and J. Stefels. 2007. Photosynthetic responses in *Phaeocystis antarctica* towards varying light and iron conditions. *Biogeochemistry* **83**: 61–70.
- van Leeuwe, M. A., R. J. W. Visser, and J. Stefels. 2014. The pigment composition of *Phaeocystis antarctica* (Haptophyceae) under various conditions of light, temperature, salinity, and iron. *J. Phycol.* **50**: 1070–1080. doi:10.1111/jpy.12238
- van Leeuwe, M. A., L. Tedesco, K. R. Arrigo, P. Assmy, K. Campbell, K. M. Meiners, J.-M. Rintala, and V. Selz. and others 2018. Microalgal community structure and primary production in Arctic and Antarctic sea ice: A synthesis. *Elem. Sci. Anth.* **6**: 4. doi:10.1525/elementa.267
- Venables, H. J., A. Clarke, and M. P. Meredith. 2013. Winter-time controls on summer stratification and productivity at the western Antarctic Peninsula. *Limnol. Oceanogr.* **58**: 1035–1047. doi:10.4319/lo.2013.58.3.1035
- Vernet, M., D. Martinson, R. Iannuzzi, S. Stammerjohn, W. Kozłowski, K. Sines, R. Smith, and I. Garibotti. 2008. Primary production within the sea-ice zone west of the Antarctic Peninsula: I-Sea ice, summer mixed layer, and irradiance. *Deep. Res. Part II Top. Stud. Oceanogr.* **55**: 2068–2085. doi:10.1016/j.dsr2.2008.05.021
- Webb, A. L., M. A. van Leeuwe, D. den Os, M. P. Meredith, H. Venables, and J. Stefels. 2019. Extreme spikes in DMS flux double estimates of biogenic sulfur export from the Antarctic coastal zone to the atmosphere. *Nature Sci. Rep.* **9**: 2233. doi:10.1038/s41598-019-38714-4
- Wright, S. W., D. P. Thomas, H. J. Marchant, H. W. Higgins, M. D. Mackey, and D. J. Mackey. 1996. Analysis of phytoplankton of the Australian sector of the Southern Ocean: Comparisons of microscopy and size frequency data with interpretations of pigment HPLC data using the CHEMTAX matrix factorisation program. *Mar. Ecol. Prog. Ser.* **144**: 285–298.
- Wright, S. W., R. L. van den Enden, I. Pearce, A. T. Davidson, F. J. Scott, and K. J. Westwood. 2010. Phytoplankton community structure and stocks in the Southern Ocean (30–80°E) determined by CHEMTAX analysis of HPLC pigment signatures. *Deep Res. Part II* **57**: 758–778. doi:10.1016/j.dsr2.2009.06.015
- Xu, K., F.-X. Fu, and D. A. Hutchins. 2014. Comparative responses of two dominant Antarctic phytoplankton taxa to interactions between ocean acidification, warming, irradiance, and iron availability. *Limnol. Oceanogr.* **59**: 1919–1931.
- Zhu, Z., K. Xu, F. Fu, J. L. Spackeen, D. A. Bronk, and D. A. Hutchins. 2016. A comparative study of iron and temperature interactive effects on diatoms and *Phaeocystis antarctica* from the Ross Sea, Antarctica. *Mar. Ecol. Prog. Ser.* **550**: 39–51.
- Zhu, Z., P. Qu, J. Gale, F. Fu, and D. A. Hutchins. 2017. Individual and interactive effects of warming and CO<sub>2</sub> on *Pseudonitzschia curvata* and *Phaeocystis antarctica*, two dominant phytoplankton from the Ross Sea, Antarctica. *Biogeochemistry* **14**: 5281–5295.

#### Acknowledgments

We thank the Dutch Program winter research assistants Amber Annett, Mairi Fenton and Emily Davey for collecting samples over winter. We are grateful to the technical staff at the British Antarctic Survey Rothera Station for all general support. We thank Janne-Markus Rintala for microscopic analyses and the Royal Netherlands Institute for Sea Research for nutrient analyses. Funding for this study was provided by the Netherlands Organisation for Scientific Research (NWO) under the Polar Program (NPP) Project Numbers 866.10.101 and 866.14.101. RaTS is a component of the BAS Polar Oceans research program, funded by the U.K. Natural Environment Research Council.

#### Conflict of Interest

None declared.

Submitted 12 April 2019

Revised 20 January 2019

Accepted 15 May 2020

Associate editor: Anya Waite